Dispersion relations of longitudinal and transverse waves in two-dimensional screened Coulomb crystals

S. Nunomura,* J. Goree,† S. Hu, X. Wang,‡ and A. Bhattacharjee
Department of Physics and Astronomy, The University of Iowa, Iowa City, Iowa 52242
(Received 18 May 2001; revised manuscript received 19 February 2002; published 12 June 2002)

Dispersion relations of longitudinal and transverse waves in two-dimensional (2D) screened-Coulomb crystals were investigated. The waves were excited in 2D crystals made from complex plasmas, i.e., dusty plasmas, by applying radiation pressure of laser light. The dependencies of the dispersion relation on the shielding parameter, the damping rate, and the wave propagation direction were experimentally measured. The measured dispersion relations agree reasonably with a recently developed theory, and the comparison yields the shielding parameter and the charge on particles.

DOI: 10.1103/PhysRevE.65.066402 PACS number(s): 52.27.Lw, 82.70.Dd, 52.35.Fp, 52.27.Gr

I. INTRODUCTION

A screened Coulomb system is a collection of particles interacting through a shielded Coulomb potential. For a point particle of charge Q, the interaction potential is the Yukawa potential $V(r)$, which is defined by

$$V(r)=\frac{Q}{4\pi\varepsilon_0 r}\exp\left(-\frac{r}{\lambda_D}\right). \tag{1}$$

Here, r is the distance from a charged particle and λ_D is the shielding length. When the system is in thermodynamic equilibrium, it is characterized by two parameters: the shielding parameter κ and the Coulomb coupling parameter Γ. These parameters are expressed as

$$\kappa=\frac{a}{\lambda_D}, \tag{2}$$

$$\Gamma=\frac{Q^2}{4\pi\varepsilon_0 a k_B T}, \tag{3}$$

where a is the mean interparticle spacing and T is the kinetic temperature of the particles. The system is classified as ''strongly coupled'' or ''weakly coupled,'' for $\Gamma\geqslant 1$ or $\Gamma\ll 1$, respectively. When $\Gamma\gg 1$, the system can be in a solid state, where it usually has an ordered structure such as bcc and fcc, depending on κ and Γ [1]. In the limit of $\kappa=0$, i.e., a one-component plasma, the critical value of Γ for the transition between a liquid and solid state is known to be approximately 170 [1–4]. The screened Coulomb system has a triple point, i.e., the intersection of fluid-solid and solid-solid phase boundaries, which is known to be at $\kappa=4.28$ and $\Gamma=5.6\times 10^3$ [1].

Within a screened Coulomb crystal, two kinds of wave modes exist: longitudinal and transverse waves. The longitudinal wave is a compressional wave that propagates parallel to the particle motion in the medium. The transverse wave, also known as the shear wave, propagates perpendicular to the particle motion. It is known that the longitudinal wave can propagate in all states of the screened Coulomb system (gas, liquid, and solid); however, the transverse wave propagates only in the strongly coupled regime, i.e., liquid and solid states.

A two-dimensional (2D) crystal is the system we consider in this paper. One of the distinctions of waves in a 2D lattice is that the sound speed depends on κ more weakly than for a three-dimensional (3D) lattice. For the longitudinal mode at $\kappa\ll 1$, Wang *et al.* [5] found that the sound speed is proportional to κ^{-1} for a 3D triangular lattice, to $\kappa^{-1/2}$ for a 2D triangular lattice, and to $(-\ln\kappa)^{1/2}$ for a one-dimensional (1D) chain. This is primarily because the number of particles interacting with one another depends on the geometry.

Two examples of screened Coulomb systems are complex plasmas (often called dusty plasmas) and colloidal suspensions. A main difference between these two systems is the damping rate for particle dynamics. Since colloidal suspensions are generally produced in liquid electrolytes, particle motion is strongly restricted due to the large friction with the background liquid medium. However, in complex plasmas, the particles are immersed in a rarefied gas, which exerts a much weaker damping.

A complex plasma is an ionized gas containing small particles of solid matter. It usually consists of four components: electrons, ions, particles, and gas molecules. Particles in plasmas are usually negatively charged due to the higher mobility of electrons as compared to ions. For example, the charge on a micron-sized sphere immersed in a plasma with an electron temperature of a few eV is thousands of electrons. Therefore, the particles can affect each other through a strong electrostatic repulsion, which leads the system to be strongly coupled [6]. In such a situation, the particles may organize themselves into a lattice, i.e., an ordered structure, called a plasma crystal [7–10].

The electrons and ions in the plasma serve the roles of charging the particles and shielding the electrostatic field around the particles. The gas discharge used in experiments also includes gas molecules, because the gas is only weakly ionized. The gas cools the particles to a particle kinetic tem-

*Present address: Max-Plank-Institut für Extraterrestrische Physik, D-85740 Garching, Germany.
†Email address:
‡Permanent address: Department of Physics, Dalian University of Technology, Dalian, China 116024.

perature as low as the gas temperature. The damping of particle motion due to collisions with gas molecules is characterized by the Epstein drag coefficient ν_E, which is expressed as

$$\nu_E = \delta \sqrt{\frac{8m_g}{\pi k_B T_g}} \frac{p}{\rho r_p}, \tag{4}$$

where p is the gas pressure, m_g and T_g are the mass and temperature of gas molecules, and r_p and ρ are the radius and the material density of the particles, respectively. In Epstein theory [11], the leading coefficient δ ranges from 1.0 in the case of specular reflection to 1.44 for diffuse reflection. Here we assume 1.44. Typical values of ν_E for micron-sized particles are of the order of 1 s^{-1} for a gas pressure $p \sim 10$ mTorr. This is smaller than in colloids by a factor of $\sim 10^3$.

There have been several wave experiments reported for complex plasmas. In a strongly coupled regime, Pieper and Goree [12] excited longitudinal waves in a multilayer lattice with a relatively high gas pressure, using an electrostatic excitation scheme. Homann *et al.* [13] excited the same kind of waves in a 1D chain and 2D crystal, but using laser manipulation. Here, we also use laser manipulation to launch waves in our crystals. The transverse mode was recently observed by Nunomura *et al.* in a 2D crystal [14] and Misawa *et al.* in a 1D chain [15]. However, we know of no wave experiments until now, where both the longitudinal and transverse modes were excited under the same experimental conditions.

In this paper we present dispersion relations of both wave modes measured in 2D plasma crystals, and we compare the results with theoretical dispersion relations. Dependencies of the dispersion relations on κ, the damping rate, and the direction of wave propagation are comprehensively investigated. We propose two diagnostic methods for κ and Q, using dispersion relation measurements of both modes and sound speeds.

II. THEORY OF DISPERSION RELATIONS

Dispersion relations for longitudinal and transverse modes have been theoretically developed in screened Coulomb systems using two approaches. First, the hydrodynamic approach is useful for gas and liquid phases because the kinetic effects, i.e., particle thermal motions, play an important role in wave propagation. Second, one can directly solve the equation of motion; this can be done analytically for the solid phase, or using molecular dynamics (MD) simulation for all phases.

For a liquid state, Kaw and Sen [16] developed dispersion relations using the generalized hydrodynamic equations, where they used a nonlocal viscoelastic operator to account for the memory effect and short range order. Latter, Kalman *et al.* [17] also derived dispersion relations, but from a different approach, using the quasilocalized charge approximation method. Molecular dynamics simulations were recently carried out to investigate the detail of dispersion characteristics [18]. The theories and simulation results predict that in a liquid there is a critical wave number, below which shear waves cannot be sustained. The reason is thought to be that long-range correlation diminishes in a liquid state because of kinetic effects.

For a solid state, Peeters and Wu presented a phonon spectrum, i.e., a dispersion relation, of a 2D hexagonal crystal [19]. They carried out a numerical calculation of the dynamical matrix of the crystal, which ignores kinetic effects and damping. In our previous work on the transverse mode [14], we used this dispersion relation to compare with experimental results. Unfortunately, it did not allow us to compare the imaginary part of the wave number because the theory did not take damping into account. In a 1D lattice, dispersion relations were analytically derived by Melandsø for the longitudinal mode [20] and Vladimirov *et al.* for the transverse mode [21].

In this paper we compare experimental results to the recently developed dispersion relations of Wang *et al.* [5]. They derived the dispersion relations of both modes from a unified perspective by solving the linearized equation of motion analytically. Their theory is basically applicable to strongly coupled screened Coulomb crystals in all dimensions, and in a 2D triangular lattice it is similar to the theory of Dubin [22]. It is possible to adopt the theory to another kind of interaction potential, by choosing an appropriate spring constant matrix expression. Here, we only describe the theory for a 2D triangular screened Coulomb lattice with hexagonal symmetry, in which wave damping is included. In real experiments, the differences from the assumptions of the theory are as follows: the existence of particle thermal motion, defects, and particle size dispersion. Other differences from theory, which we believe are insignificant, include nonlinear particle interaction and gradients in the particle number density due to the influence of gravity and the sheath.

For waves propagating parallel to one of the primitive translation vectors, the dispersion relations for both longitudinal and transverse modes are expressed, respectively [Eqs. 6(a) and 6(b) in Ref. [5]], as

$$\omega_l(\omega_l + i\nu) = 2\sum_{x,y} F(X,Y)\sin^2\left(\frac{kX}{2}\right), \tag{5a}$$

$$\omega_t(\omega_t + i\nu) = 2\sum_{x,y} F(Y,X)\sin^2\left(\frac{kX}{2}\right), \tag{5b}$$

where the summation is carried out all over the particles in the 2D lattice, and ν represents the frictional drag coefficient. The frequencies ω and ν are normalized by ω_0, and equilibrium particle position X, Y, and k are normalized by a. Here, ω_0 is defined as

$$\omega_0 = \sqrt{\frac{Q^2}{4\pi\varepsilon_0 m a^3}}, \tag{6}$$

where m is the mass of a particle. This resembles the expression for a plasma frequency. The function $F(X,Y)$ represents the spring constant matrix, which is given by

$$F(X,Y)=R^{-5}e^{-\kappa R}[X^2(3+3\kappa R+\kappa^2R^2)-R^2(1+\kappa R)], \tag{7}$$

where $R^2=(X^2+Y^2)$.

According to the theory, wave dispersion relations depend on three parameters: κ, ν, and the direction of wave propagation as compared to the crystal alignment. Wang *et al.* [5] and Dubin [22] found that both the longitudinal and transverse waves had a nondispersive character, i.e., $\omega \propto k$ for small values of k. The slope of the ω vs k curve, where it is straight, is a sound speed. They found that the sound speed was independent of the propagation direction, for both modes. As the wavelength becomes shorter, ω is no longer proportional to k, and then the dispersion relation depends on the propagation direction.

III. METHOD OF WAVE EXPERIMENT AND ANALYSIS

We performed wave experiments in a 2D triangular lattice with hexagonal symmetry. The lattice was formed by levitating a single horizontal layer of particles in the plasma sheath. A schematic view of experimental apparatus is shown in Fig. 1(a). The same apparatus was used earlier for a previous series of transverse wave experiments [14].

An argon plasma was generated by a capacitively coupled rf discharge operated at 13.6 MHz at a gas pressure of 18.6–33.6 mTorr. The various discharge conditions in which we performed wave experiments are listed in Table I. We chose a relatively low gas pressure in order to reduce the gas friction damping of the waves. The lower electrode was driven by rf power with a peak-to-peak voltage $V_{pp}\sim 60$ V, using a matching network. In order to characterize plasma parameters in the main plasma, we made Langmuir probe measurements, and we found that typically $T_e\sim 1$ eV, $n_e=3-6\times 10^8$ cm^{-3}, and the plasma potential $V_s\sim 20$ V. We checked that the plasma parameters in the main plasma did not change much when particles were introduced. On the lower electrode, a self-bias voltage appeared, which helps levitate particles. It varied from $V_b=-30$ V to -40 V, depending on p and V_{pp}.

A 2D plasma crystal was made by introducing microspheres into plasma. The particles are polymer spheres of mean radius $r_p=4.04$ μm, and their size distribution has a standard deviation of 0.09 μm. Their mass density is 1.51 g/cm^3, corresponding to $m=4.17\times 10^{-13}$ kg. After particles were dispersed into the plasma, some of the particles were trapped in the plasma sheath area above the horizontal lower electrode. A weak radial electrostatic field in the plasma confined the particles in the radial direction. Due to a combination of this confinement and the interparticle repulsion, particles organized themselves into a monolayer triangular lattice with hexagonal symmetry. The crystal was $\sim$7 cm in diameter, and it included 3000–10 000 particles. By adding or removing particles, we adjusted the number density of particles in a monolayer crystal, allowing us to control κ. By doing this, the interparticle spacing was changed from $a=0.67$ to 1.3 mm, corresponding to a change of approximately a factor of 2 in κ. In our experiment, the crystal spontaneously rotated as a rigid body in a horizontal plane at a constant angular speed of ~ 30 °/min, which is much slower than the wave propagation speed of either mode. The cause of this spontaneous rotation is unclear, but it proved to be useful because it allowed us to measure the dispersion relations at various wave propagation directions with respect to the primitive translation vectors of the lattice.

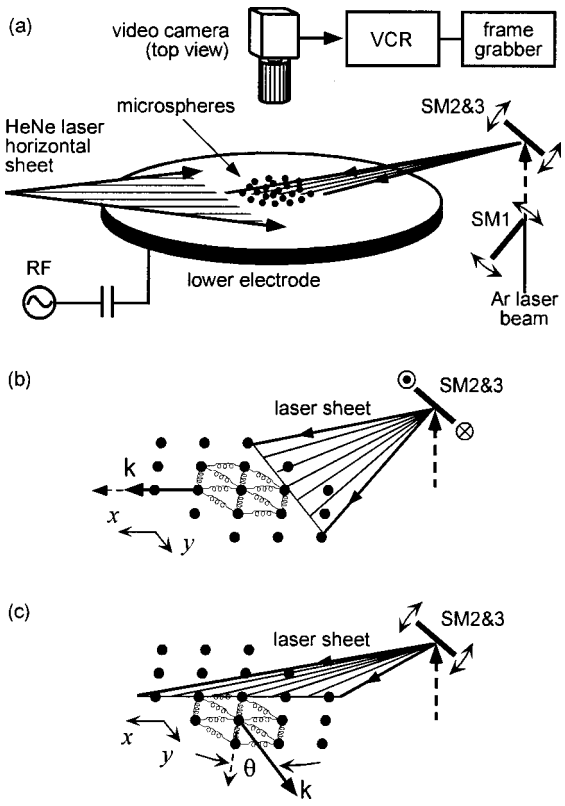

FIG. 1. (a) Sketch of experimental apparatus. A wave was excited by applying an intensity-modulated laser sheet to a 2D plasma crystal. Microspheres were levitated in the plasma sheath above the lower electrode, and they formed an ordered structure, a so-called ''plasma crystal.'' (b) and (c) Method of wave excitation for both the longitudinal and the transverse modes. A laser sheet expanded in the y direction was used for a longitudinal wave excitation. To launch a transverse wave, the laser sheet was spread in the x direction. The direction of wave propagation was defined as the angle θ with respect to one of the primitive translation vectors.

Particles were imaged by a charge-coupled device (CCD) video camera located above the crystal. The particles in a 2D crystal were illuminated with a horizontal He-Ne laser sheet with a power small enough that it did not move the particles. The camera was equipped with a microlens and a He-Ne interference filter. The field of view was 24×18 mm, and it included 300–1100 particles. Images were recorded on an SVHS videocassette recorder (VCR) tape at 30 frames per second.

We used the radiation pressure of an Ar laser sheet to launch a plane wave in the 2D crystal. By changing the orientation of the laser sheet, we were able to excite either a longitudinal or transverse wave. Three galvanometer-scanning mirrors (SM1, SM2, and SM3, shown in the right side of Fig. 1) were employed to control the wave frequency and the wave mode, i.e., a longitudinal or transverse wave.

TABLE I. Discharge conditions and plasma parameters in main plasma.

Quantity	Unit	Experimental No. I	II	III	IV	V	VI	VII	VIII	IX
Discharge conditions										
P	mTorr	18.6	18.6	18.6	18.6	18.6	18.6	23.6	28.6	33.6
V_{pp}	V	62	62	62	62	62	62	60	61	62
V_b	V	−40	−40	−40	−40	−40	−40	−37	−31	−30
Plasma parameters										
T_e	eV		1.2	1.1	1.0	1.0	1.0	1.2	0.8	0.8
n_e	10^8 cm^3		3.0	3.5	3.4	3.6	3.2	3.5	5.8	5.8
V_s	V		20	21	20	20	20	21	21	21

The procedure for wave excitation was as follows. Mirror SM1 determined the wave frequency by chopping the laser beam. The driving frequency was varied up to several Hz. The chopping was not a square wave; instead, we applied a smoother wave form to SM1, yielding a nearly sinusoidal modulation of the laser power. The second and third harmonics had a power of typically only 3% of the fundamental, and higher harmonics were too small to measure. After the laser beam was modulated, the beam was focused by a telescope. At the crystal, the Gaussian full width at half maximum (FWHM) was 0.7 mm. Then, the focused laser beam was deflected by mirrors SM2 and SM3. One of the two mirrors was stationary while the other formed a laser sheet by oscillating at 300 Hz. Note that this frequency is two orders of magnitude higher than the wave driving frequency; the particles are too massive to respond to a stimulation at 300 Hz. Next, the laser sheet struck the crystal at a grazing angle of 10°, so that it applied its momentum mainly in the horizontal direction. From images of the side view of the crystal, we checked that particles did not move in a vertical direction when the laser sheet irradiated them, i.e., their motion was strictly 2D. The Ar laser power was adjusted to be relatively low for three reasons: to suppress secular drift in the crystal, to avoid disturbing the crystal structure, and to avoid nonlinear wave motion. In the experiments, we applied a laser power of 0.5 W distributed in a sheet slightly wider than the crystal diameter.

Here we define the x axis as parallel to the direction of longitudinal wave propagation, and the y axis is the direction of transverse wave propagation. To excite a longitudinal wave, the Ar laser sheet was expanded in the y direction, as shown in Fig. 1(b). In contrast, the Ar laser was expanded in the x direction to launch the transverse wave Fig. 1(c). The particle motion in both waves was always in the x direction. The wave propagation direction was defined by the angle θ with respect to one of the primitive translation vectors.

In order to obtain the wave dispersion relation, we analyzed particle motion. Our method, which was introduced in Refs. [14,23], was as follows. First, video images were digitized with an 8-bit gray scale and a 640×480 pixel resolution. The frame rate for digitized images was chosen in the range of 10 to 30 frames per second, to include several periods of wave motion. Then, individual particles were identified as contiguous pixels that have a brighter intensity than the threshold value. By weighting the brightness over contiguous pixels, the center of a particle was calculated, with subpixel resolution, in x-y coordinates. Each particle's trajectory was obtained by tracing its position from one frame to another over a total of 128 frames, corresponding to 4.2–12.7 s, depending on the wave excitation frequency. At the same time, the particle velocity was also calculated from the difference of particle position in consecutive two frames. Next, depending on the equilibrium particle position, particles were divided into 40 bins, i.e., stripes aligned perpendicular to the wave propagation direction. The particle position and velocity were averaged in each bin, yielding a time series of velocity for each bin. After that, the wave amplitude and phase were obtained from a temporal Fourier transform of particle motion associated with the fundamental frequency. We used the particle velocity, not the particle position, as the input for this Fourier transform to eliminate the effect of any secular particle drift. Finally, the real and imaginary parts of the wave number were obtained by fitting the phase shift and amplitude decay of the wave as functions of distance, as explained in the next section.

IV. RESULTS OF WAVE EXPERIMENTS

A. Crystal structure

An image of a typical 2D crystal is shown in Fig. 2. The image has been thresholded and inverted, so that particles appear as black spots. The upper right image is an enlargement of part of the crystal, showing a triangular lattice with hexagonal symmetry. To obtain the interparticle spacing a

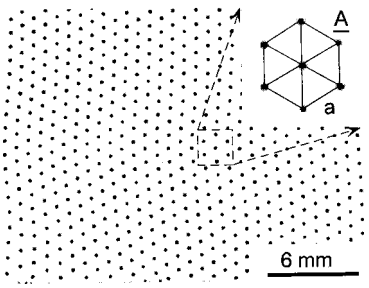

FIG. 2. Image of a 2D plasma crystal. The inset is an enlargement of a part of the image, where we have also drawn lines to show the triangular lattice with hexagonal symmetry.

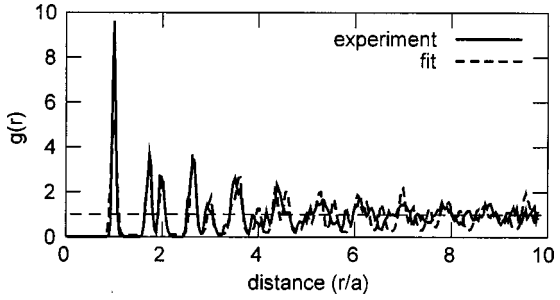

FIG. 3. Pair correlation function $g(r)$. The large number of peaks indicates a long-range translational order.

and evaluate the crystal ordering, the pair correlation function $g(r)$ was calculated. Figure 3 is an example of $g(r)$. In our experiments, typically, a was $\sim$1 mm and the translational correlation length [24] was several times lager than a. The presence of many peaks in $g(r)$ indicates a long-range translational order.

B. Phase and amplitude of wave

To obtain both parts of the wave number $k=k_r+ik_i$, we calculated the phase shift and the amplitude decay of wave from analyzing particle motions. Here, we show examples for both the transverse and longitudinal modes, because the amplitude decay is different.

For the transverse mode, the phase shift and amplitude decay were as expected. Figure 4(a) clearly shows that the phase is proportional to the distance from the wave excitation source at $y=0$. By fitting it as a linear function, the slope yields k_r. For a mode of high ω, the slope is steep corresponding to a short wavelength. The wave amplitude A decays exponentially as the wave propagates. This is shown in Fig. 4(b), which is plotted with semilogarithmic axes. The amplitude decay is fit to an exponential function, yielding k_i. In experiments, the typical wave amplitude is a few tens of μm, corresponding to a few percent of a. The wave amplitude decreased with ω because in a period of wave motion, the momentum supplied by the laser radiation decreased with ω.

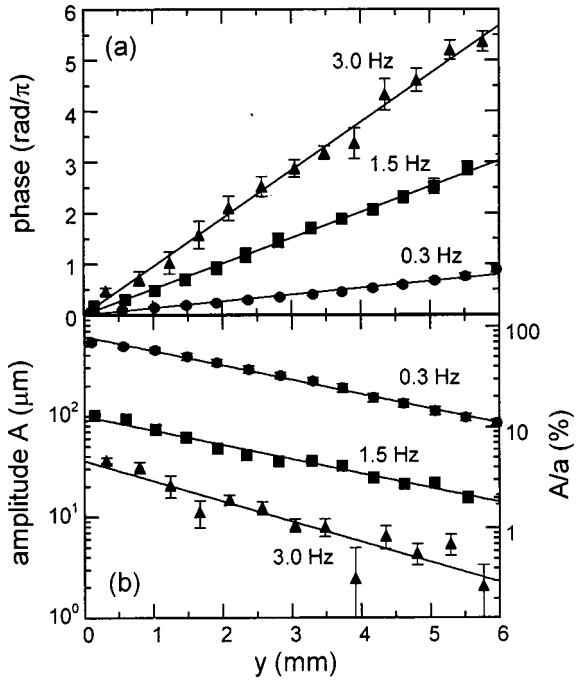

FIG. 4. (a) Phase shift and (b) amplitude decay for transverse waves. The linear slope in phase and exponential decay in amplitude give k_r and k_i, respectively. Solid lines are fits. The waves were launched at $y=0$.

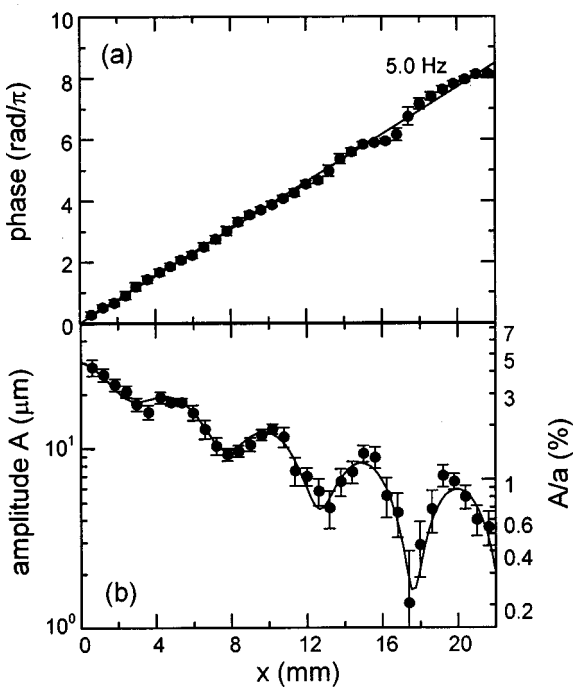

FIG. 5. (a) Phase shift and (b) amplitude decay, for a longitudinal wave. The amplitude decay includes a beat structure, which we explain as a superposition of a sloshing mode and a longitudinal wave. Solid curves are fits, yielding k_r and k_i. The wave excitation is at $x=0$.

Since the wave amplitude is small, the waves were believed to be linear. In a test, we verified that the wave amplitude varied linearly with the laser power up to 0.7 W, a range that includes the laser power used for the wave excitation presented in this paper. As a further test of nonlinearity, we measured the harmonics present in the wave spectrum. The harmonics were weak, and possibly originated from our imperfect sinusoidal modulation of the laser power. For example, the amplitude of the third harmonics was $<$10% of the fundamental.

The amplitude decay of the longitudinal mode exhibited an unexpected feature. In Fig. 5 the phase and amplitude decay for the longitudinal mode is shown, where the phase varies linearly with the distance that the wave has propagated. Fitting this to a straight line yields k_r, which for this example corresponds to a wavelength of 5 mm. The amplitude decay in Fig. 5(b), however, was not a simple exponential decay; it included a beat structure. We found that the beat

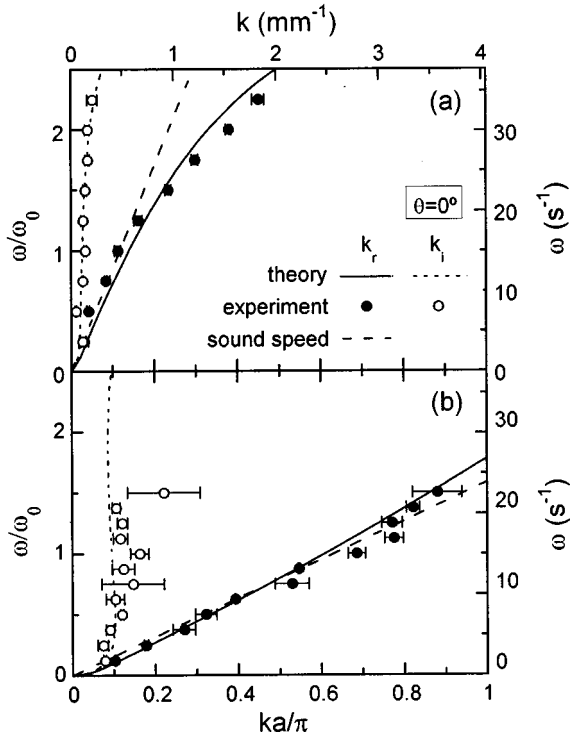

FIG. 6. Dispersion relations of (a) the longitudinal and (b) the transverse waves. A dispersive characteristic is shown for the longitudinal wave at high ω while the transverse wave remains a linear relationship $\omega \propto k_r$ over a wide range of k_r. The data were obtained at $\theta = 0°$ in Experiment II (see Tables I and II). The closed and open circles are experimental data for k_r and k_i, respectively. The solid and dashed curves are k_r and k_i, calculated from the theory of Wang *et al.* [5]. The broken lines are sound speeds obtained from fitting experimental data less than $\omega/\omega_0 < 1$; C_l is faster than C_t. For comparison, both dispersion relations are plotted in same scale with normalized axes ω/ω_0 and ka/π, where $ka/\pi = 1$ corresponds to the wavelength of $2a$. The upper horizontal and the right vertical axes are labeled in real values.

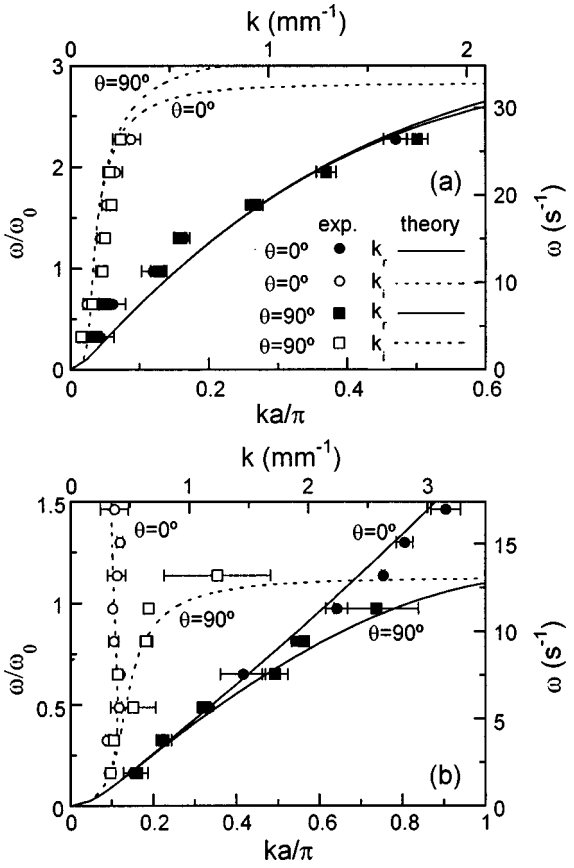

FIG. 7. Comparison of dispersion relations for two directions θ of wave propagation. The longitudinal mode does not strongly depend on θ, as shown in (a). The transverse mode, however, is sensitive to θ, especially for high ω, as shown in (b). The data were measured at $\theta = 0°$ and 90° in Experiment III.

spacing corresponds to the wavelength of the longitudinal wave obtained from linear fitting of the phase shift. From the lower figure, the beat spacing is estimated to be 5 mm, comparable to the wavelength determined from the phase plot.

Here, we explain the beat structure in the amplitude decay. We know that the beat cannot be explained as a reflected longitudinal wave because the beat spacing $2\pi/k_r$ is not π/k_r as would be expected for the interference of two waves of the same wavelength. Instead, the beat spacing is consistent with the interference of the longitudinal wave with another disturbance having the same frequency, but a much longer wavelength.

The lattice structure can oscillate several ways in addition to the longitudinal and transverse modes. One way is the ''sloshing'' mode, where the entire lattice oscillates as a rigid body, like a pendulum in an external confining potential corresponding to our radial electric field. Even a local disturbance like our laser beam can cause the entire body to be displaced, because the lattice is crystalline and therefore can move as a rigid body. Superposing the longitudinal wave with amplitude A_0 and a sloshing mode with amplitude B_0, the particle displacement $f(x)$ is

$$f(x) = A_0 \cos(\omega t - k_r x)\exp(-k_i x) + B_0 \cos(\omega t). \quad (8)$$

Performing a Fourier transform of Eq. (8) yields a fitting function $A(x)$ for the amplitude decay:

$$A(x) = A_0 \sqrt{\left(\frac{B_0}{A_0}\right)^2 + 2\left(\frac{B_0}{A_0}\right)\cos(k_r x)\exp(-k_i x) + \exp(-2k_i x)}. \quad (9)$$

TABLE II. Characteristic parameters of crystals.

		Experiment No.								
Quantity	Unit	I	II	III	IV	V	VI	VII	VIII	IX
					Pair correlation function					
a	mm	0.67	0.78	0.90	1.00	1.10	1.32	0.93	0.87	0.85
					Wave dispersion relations					
κ		0.9	1.0	1.2	1.3	1.4	1.5	1.0	1.0	0.9
ω_0	s^{-1}	20.1	15.1	11.6	9.8	8.5	5.6	10.7	10.8	10.6
Q	$10^4 e$	1.5	1.4	1.3	1.3	1.3	1.1	1.3	1.2	1.1
					Wave damping					
ν_E/ω_0		0.19	0.25	0.32	0.38	0.44	0.67	0.44	0.53	0.64
$\nu_{\rm fit}/\omega_0$		0.27	0.36	0.39	0.46	0.53	0.81	0.67	0.63	0.68
					Particle velocity distribution					
T	eV	0.107	0.037	0.038	0.030	0.031	0.045	0.031	0.037	0.034
Γ		4400	9700	7500	8500	7400	3100	8400	6400	6200
$\Gamma \exp(-\kappa)$		1800	3600	2300	2300	1800	700	3100	2300	2500

There are four free parameters in Eq. (9) to fit the amplitude decay: A_0, B_0, k_r, and k_i. However, we reduced the free parameters to three by substituting k_r obtained from the phase plot. The solid curve in Fig. 5(b) is a fit calculated from Eq. (9), which gives a good agreement with experimental data points. From this fit, we found k_i for the longitudinal mode.

From the amplitude decay fit, we were also able to estimate B_0. The amplitude B_0 indicated a tendency to decrease with ω for the longitudinal wave excitation. However, B_0/A_0 remained almost the same, roughly 0.1 for all the conditions we used.

C. Dispersion relations

The dispersion relations of both modes were measured at various values of θ, κ, and ν. To clarify the difference of dispersion relations based on the wave propagation direction, we measured them at two distinctive angles, $\theta=0°$ and 90°, with respect to the primitive translation vector. For measuring κ dependence, the number density of particles in the 2D crystal was changed under the same discharge conditions. The range of κ was varied as much as possible, 0.9 to 1.5. We also performed wave experiments at different values of gas pressure to study how the gas friction affects the wave damping. The normalized friction coefficient ν/ω_0 was changed from 0.27 to 0.68.

One of our chief results is a dispersion relation for both wave modes, measured for the same conditions, as shown in Fig. 6. The transverse wave was dispersionless, i.e., $\omega \propto k_r$, over a wider range than for the longitudinal wave. The latter exhibits dispersion, i.e., ω vs k_r is a curved line, for $\omega > \omega_0$. Looking at the slope of the dispersion relation at $k_r = 0$, which defines the sound speed, we notice that the sound speed C_l of the longitudinal mode is faster than C_t of transverse modes as expected. In our experiments the sound speed is a few cm/s for the longitudinal mode and several mm/s for the transverse mode, respectively. The ratio of C_l/C_t is approximately 5, for $\kappa \sim 1$. The wave frequency and wavelength are typically a few Hz and several mm, respectively, for both modes.

Comparing measured and theoretical dispersion relations, we find a reasonable agreement over the range $0 < k_r a/\pi < 0.6$ for the longitudinal mode and $0 < k_r a/\pi < 1$ for the transverse mode. Since we do not know the actual values of κ, ν, and ω_0 in the experiment, we allowed them to be free parameters when fitting the theoretical curves to the experimental results. As initial estimates in the fit parameters, we used $\kappa=1$, Epstein drag for $\nu_{\rm fit}$, and ω_0 as calculated from C_t as discussed later. The resulting values of κ, $\nu_{\rm fit}$, and ω_0, consequently Q, are listed in Table II.

The theory predicted that the dispersion relation is anisotropic, i.e., the dispersion relations varies with θ [5,19,22]. We verified this experimentally. Figure 7 shows two kinds of dispersion relations at $\theta=0°$ and 90°. For long wavelengths, the dispersion relations are independent of θ. However, for small wavelengths, typically $k_r a/\pi > 0.5$, the dispersion relation is sensitive to θ, especially for the transverse wave.

The dispersion relations also depend on κ. Figure 8 shows results for the κ dependence of the dispersion relations. The sound speeds of both modes decrease with κ, i.e., they increase with the number density of particles. This result can be understood intuitively because particles that are spaced more closely will interact with greater force. The same data are shown with normalized axes in Fig. 9. We also note that the wave damping of longitudinal modes increased with κ.

The friction coefficient ν, as a parameter in the dispersion relation, influences k_i more than k_r, for a given value of ω. The way that the wave damping increases with ν is shown by experimental data in Fig. 10. In this comparison, we chose the same value of $\kappa \sim 1$, for both the large and small ν cases, to eliminate the κ dependence of wave damping. In our conditions, wave damping was not so strong, i.e., $k_i \ll k_r$.

Here, we summarize our results for dispersion characteristics, verified from comparing experimental results with theory. The experimentally measured dispersion relations agreed with the dispersion relations in a range $0.9 < \kappa < 1.5$

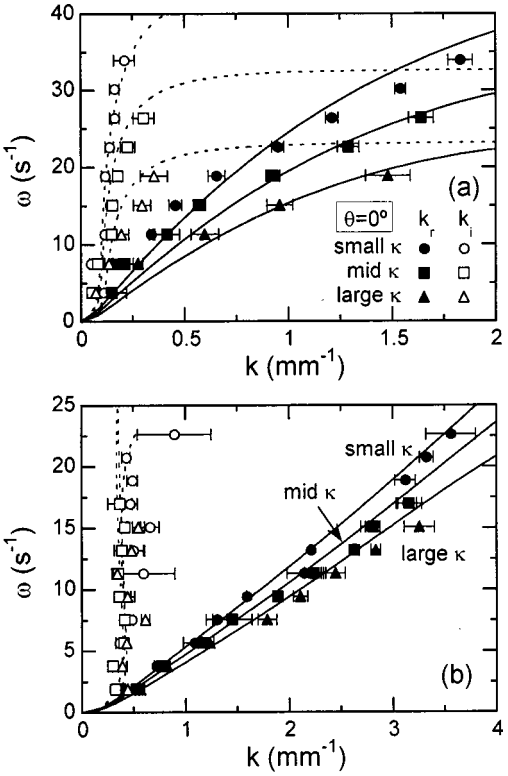

FIG. 8. κ dependence of dispersion relations. The slope at $k_r=0$, i.e., the sound speed increases with decrease of κ, for each mode. Both the dispersion relations for the longitudinal (a) and transverse mode (b) were measured at $\theta=0°$ in Experiments II, III, and V for small, medium, and large values of κ.

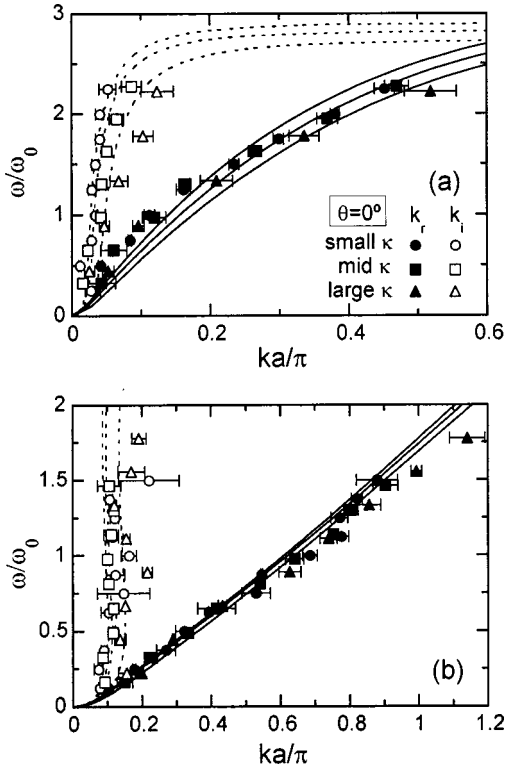

FIG. 9. κ dependence of dispersion relations. The same data as Fig. 8 are shown here, normalized by ω_0 for ω, and π/a for k. Increasing κ enhances a decay of the wave amplitude.

and $0.27<\nu/\omega_0<0.68$. A dispersive characteristic for the longitudinal mode was observed above $\omega/\omega_0\sim1$, while the transverse mode remained dispersionless for $0<k_r a/\pi<1$. Comparing the sound speeds of both modes, C_l was found to be approximately five times larger than C_t for $\kappa\sim1$. As an interesting feature based on the crystal geometry, we note that the maximum possible frequency to sustain the wave was different, depending on the wave propagation direction for the transverse mode, but not for the longitudinal mode. We also demonstrated that the sound speed of both wave modes increased with a decrease of κ. For the wave damping, we verified that increasing ν and κ led to a stronger decay of the wave amplitude.

D. Wave damping

The wave damping is in rough agreement with Epstein drag, with a discrepancy of 7–50 %. The friction coefficient $\nu_{\rm fit}$, obtained from fitting of the real and imaginary parts of both dispersion relations, is listed in Table II and plotted in Fig. 11. Calculating the Epstein drag using a leading coefficient $\gamma=1.44$ for a diffuse reflection [11], we found that the fit result $\nu_{\rm fit}$ exceeds ν_E by 7–50 %. This might be caused by additional damping mechanisms, which list below. It would require a more precise measurement of gas density than ours, and measurement for multiple particle sizes, to define whether any of these effects are significant.

Generally speaking, damping mechanisms can be distinguished according to whether they apply to a single particle or only to a collective body of particles. One single-particle damping mechanism includes gas friction, i.e., Epstein drag, which is the only mechanism that has been accepted to date in the theory for the comparison with experimental data. Additional single-particle drag mechanism might include the ion drag due to the horizontal movement of particles in vertically flowing ions. Another mechanism might be resistive dissipation of electric currents corresponding to the movement of the charges induced on the surface of the electrode beneath the moving charged particles. However, our calculations suggest these mechanisms are much weaker than Epstein drag at our gas pressure. If single-particle effects were significant, they probably would have been observed in the binary Coulomb collision experiments of Konopka *et al.* [25]. However, they found that the particle damping agreed with Epstein drag, assuming a leading coefficient of $\gamma=1.48$ [26], which is only 3% larger than the value we assume.

For collective effects, we note that waves can be scattered by lattice defects or an inhomogeneity of a crystal. Thermal fluctuations of particle arrangements could also scatter the wave. One way to model this process would be a nonlinear wave-wave scattering, where the wave we excite is scattered by a zero-frequency wave corresponding to the displacements of the particles from their positions in an ideal lattice. This would result in a deflection of our wave into another direction, i.e., different **k**, but the same frequency. For example, any curvature in the rows can be modeled as a zero-

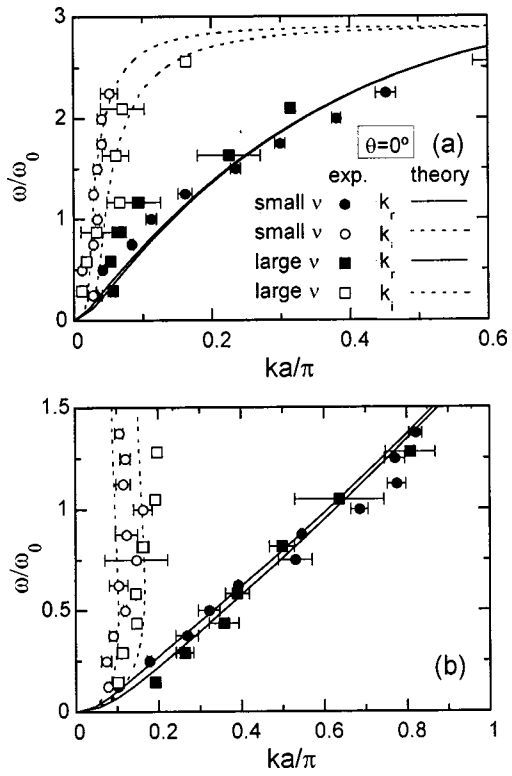

FIG. 10. Dispersion relations at different ν. The wave damping, i.e., k_i, increases with ν. To avoid the effect of varying κ, we chose the same values of $\kappa \sim 1.0$. The data were obtained at $\theta = 0°$ in Experiments II and VIII for small and large values of ν.

frequency transverse wave, and any irregular particle spacing can be modeled as a zero-frequency longitudinal wave. We would not detect the scattered wave using our present Fourier analysis technique, which resolves waves only in a single direction.

Moreover, our finite particle size dispersion of 2.2% results in a corresponding dispersion in spring constants. This dispersion is one cause of curvature of particle rows and irregular particle spacing, as discussed above. It might also directly contribute to wave scattering, which would appear as damping in our experiment.

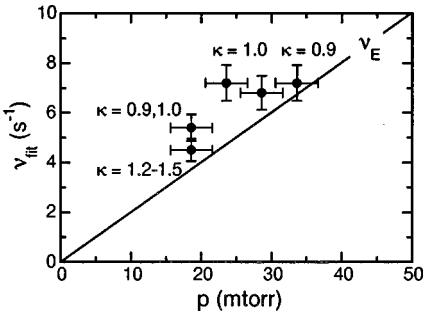

FIG. 11. Friction coefficient $\nu_{\rm fit}$ obtained from fitting the dispersion relation. The Epstein drag coefficient ν_E is shown as a solid line for reference. The observed wave damping agreed with Epstein drag within experimental uncertainty.

Another damping mechanism might include dissipation related to a delay in particle charging, i.e., ''delayed charging'' [27,28]. This dissipation mechanism is as follows. As particles approach one another in wave motion, the equilibrium charge of a particle varies because of ion orbit deflection and electron density depression. Since particle charging takes a finite time, the actual charge on a particle is different from the equilibrium value. It is known that the wave could be damped if the product of the electric field in the wave and the space derivative of equilibrium charge is positive. According to the estimate of Ivlev *et al.* [29], they expected that delayed charging plays an important role in the longitudinal mode at approximately $p < 20$ mTorr and $r_p < 1$ μm in experimental conditions similar to ours.

Resonant Landau damping, which is a process familiar to plasma physicists, is unlikely to contribute to wave damping in a crystalline lattice such as ours. This process requires that particles travel a significant distance at a constant speed that is nearly equal to the wave's phase velocity. This occurs in weakly coupled plasmas, which are gaslike, but not in strongly coupled plasmas that are crystalline. Our particles move only a distance that is small compared to the interparticle separation, and their velocity is not constant but fluctuates randomly and reverses direction frequently in response to the forces applied by neighboring particles. Moreover, our particle thermal velocity is roughly ten times smaller than the wave's phase velocity whereas resonant Landau damping in a weakly-coupled plasma requires that these velocities be nearly equal, for the damping to be strong.

V. κ AND Q DIAGNOSTICS

As mentioned in the Introduction, κ and Γ are important parameters to characterize the screened Coulomb system, and these two parameters are closely related to various fundamental phenomena such as the structure of the system, phase transition, wave propagation, and diffusion. Since Q is related to Γ through Eq. (3), κ and Q are important quantities to measure. In this section we present two diagnostic methods for measuring κ and Q, using the dispersion relations of both modes and sound speeds.

A. Dispersion relation fitting method

In a screened Coulomb crystal, the normalized dispersion relation depends on three parameters: κ, ν/ω_0, and θ as mentioned in Sec. II. Thus, fitting the dispersion relations for both modes yields values for κ, Q, and ν. Doing this required a value of a and ω_0 for the normalization of experimental values of k_r, k_i, and ω. We measured a as the first peak of pair correlation functions. From C_t, ω_0 was estimated, using

$$C_t = 0.513\ a\omega_0, \tag{10}$$

which is valid for a 2D triangular lattice with $\kappa = 0$ and $\nu = 0$ [5,19]. Equation (10) remains reasonably accurate over a wide range of κ. The sound speed of C_t varies only 20% over the range $0 < \kappa < 2$, where experiments were performed. Therefore, we relied on Eq. (10) to calculate ω_0. By using

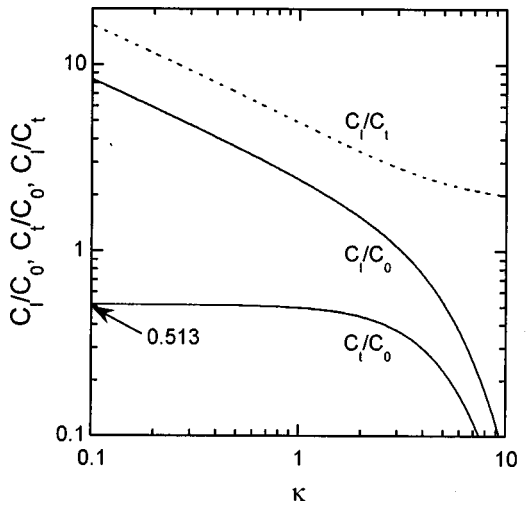

FIG. 12. C_l/C_0, C_t/C_0, and C_l/C_t vs κ in theory. A 2D triangular lattice is assumed. $C_l/C_0 \propto \kappa^{-1/2}$ and $C_t/C_0 \approx 0.513$ at $\kappa \ll 1$. These curves are useful for κ and Q diagnostics. The ratio C_l/C_t gives κ. Accordingly, Q is obtained from one of two curves C_l/C_0, C_t/C_0 through Eq. (11).

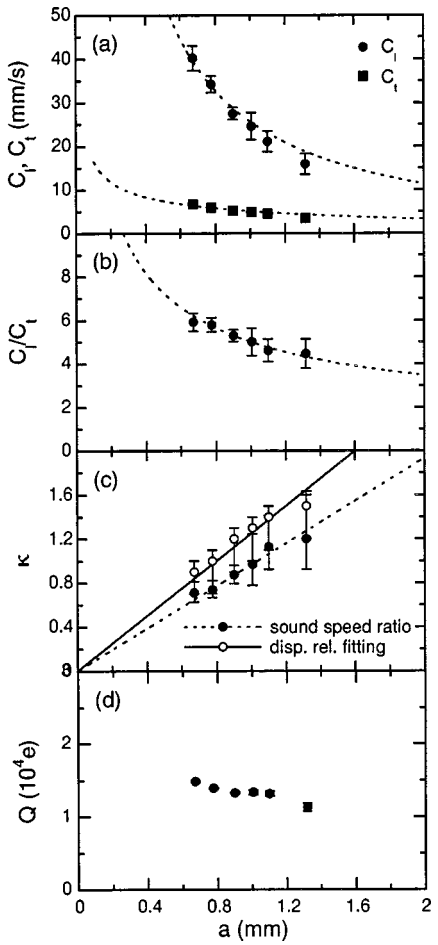

FIG. 13. (a) C_l, C_t and (b) C_l/C_t vs a in experiments. Measured C_l, C_t, and C_l/C_t fit with theory drawn as dotted curves. (c) κ measurement at different a. Closed and open circles denote values of κ obtained from the sound speed ratio and the dispersion relation fitting methods, respectively. The dotted and solid lines are linear fits of κ, yielding the shielding length λ_D. (d) Estimation of Q. As expected, Q is almost independent of a. The data were obtained in Experiments I–VI, all at the same discharge conditions.

the normalized values of $k_r a/\pi$, $k_i a/\pi$, and ω/ω_0, the free parameters to fit the dispersion relations were reduced to two: κ and ν/ω_0 because we know the wave propagation direction θ directly from the images.

The fitting for both wave modes was good over a wide range of k as shown in Figs. 6–10. This fit yielded precise values for κ and $\nu_{\rm fit}$, as listed in Table II. In our experiments, κ and Q were estimated to be 0.9–1.5 and 11 000–15 000 electrons, depending on a and discharge conditions, respectively.

We also calculated Γ as follows. From the particle velocity distribution in the crystal without wave excitation, T was obtained. This was done by fitting the particle velocity distribution as a Maxwellian distribution. Typically, T was 0.03–0.1 eV, i.e., slightly above the room temperature. This result indicates that the crystal is not in thermodynamic equilibrium with the ambient gas. Using these values, Γ and $\Gamma \exp(-\kappa)$ are estimated to be in the range 3100–9700 and 700–3600, respectively, as listed at the bottom of Table II. This large value of Γ is consistent with highly ordered crystal observed in experiment.

B. Sound speed ratio method

Next, we present another method to estimate κ and Q, using the sound speeds of both modes. For a 2D triangular lattice, the theoretical sound speeds C_l/C_0 and C_t/C_0, and the ratio C_l/C_t are shown in Fig. 12. Here, C_0 is defined by

$$C_0 = \omega_0 a = \sqrt{\frac{Q^2}{4\pi\varepsilon_0 m a}}. \tag{11}$$

The sound speeds were numerically calculated from the slope of the dispersion relation at the limit of $k_r \to 0$ [5], which are same results as those shown in Fig. 5 of Ref. [19]. According to the theory, C_l/C_0 and C_t/C_0 depend only on κ and do not depend on θ, i.e., the sound speed is the same for all wave propagation direction. It is well known that $C_l/C_0 \propto \kappa^{-1/2}$ and $C_t/C_0 \approx 0.513$ at $\kappa \ll 1$.

The method of κ and Q diagnostics is straightforward. Since C_l/C_t depends only on κ, measuring the sound speed ratio directly yields the value of κ from the curve shown in Fig. 11. To get experimental values of C_l and C_t, we fitted data points of dispersion relations as a straight line below $\omega/\omega_0 \sim 1$. After κ is determined, C_0 is calculated from one of two theoretical curves, C_l/C_0 or C_t/C_0 vs κ, as shown in Fig. 12. The resulting value for C_0 yields Q, using Eq. (11). We used C_t/C_0 because the transverse mode is dispersionless over a wider range of k_r than the longitudinal mode. The method mentioned here is convenient, but it is only valid for the case of weak wave damping, i.e., $\nu/\omega_0 \ll 1$. Since the existence of strong damping causes the relationship of ω and k_r to deviate from a linear scaling for small k_r, the sound speed can be no longer determined in such a situation.

An example of using this method is shown in Fig. 13. Here, by changing a at the same discharge conditions, the κ dependencies of C_l, C_t, and C_l/C_t are presented. We demonstrated that measured C_l, C_t, and C_l/C_t increase as a is decreased, and agree with theoretical curves shown in Figs. 13(a) and 13(b). In experiments, typical values of C_l and C_t are a few cm/s and several mm/s, respectively. Therefore, C_l/C_t is ~ 5 at $\kappa \sim 1$. In Fig. 13(c) we plot κ obtained from the two methods: the sound speed method and the dispersion relation fitting method are plotted. As we expected, κ is proportional to a. That is because the discharge conditions are the same, i.e., λ_D is the same for all of cases. This serves as evidence that the method worked reasonably well. The sound speed ratio method gives slightly smaller values of κ than those obtained from the dispersion relation fitting. The linear fitting of these data points gives λ_D, which is estimated to be 1.03 mm from the sound speed ratio method and 0.80 from the dispersion relation fitting. Finally, Q is plotted in Fig. 13(d). The calculated Q is almost the same because Q does not change much for a tenuous density of crystal while a is changed. Since $Q \propto T_e$, the slight variation of Q seems to reflect the change in T_e shown Table I.

VI. SUMMARY

We investigated the wave dispersion relations of longitudinal and transverse modes in a 2D screened Coulomb crystal. The experimental system was a monolayer plasma crystal with a triangular lattice and hexagonal symmetry. We excited both wave modes by using laser manipulation, and we measured dispersion relations for both modes for the same discharge conditions. Dependencies of dispersion relations on κ, ν, and θ were demonstrated, and they agree with the recently developed theory [5]. We also presented two diagnostic methods for measuring κ and Q, using dispersion relations of both modes and sound speeds.

ACKNOWLEDGMENTS

We thank D. Samsonov and R. A. Quinn for their assistance at the early stage of the research and F. N. Skiff, V. Nosenko and Z. W. Ma for useful discussion. We thank L. Boufendi for TEM measurement of our particle size. This work was supported by NASA, the National Science Foundation and the Department of Energy. S. N. acknowledges financial support from the Japan Society of the Promotion of Science.

[1] S. Hamaguchi, R. T. Farouki, and D. H. E. Dubin, Phys. Rev. E **56**, 4671 (1997).
[2] S. G. Brush, H. L. Sahlin, and E. Teller, J. Chem. Phys. **45**, 2102 (1966).
[3] E. L. Pollock and J. P. Hansen, Phys. Rev. A **8**, 3110 (1973).
[4] W. L. Slattery, G. D. Doolen, and H. E. DeWitt, Phys. Rev. A **21**, 2087 (1980).
[5] X. Wang, A. Bhattacharjee, and S. Hu, Phys. Rev. Lett. **86**, 2569 (2001).
[6] H. Ikezi, Phys. Fluids **29**, 1764 (1986).
[7] J. H. Chu and Lin I, Phys. Rev. Lett. **72**, 4009 (1994).
[8] H. Thomas *et al.*, Phys. Rev. Lett. **73**, 652 (1994).
[9] Y. Hayashi and K. Tachibana, Jpn. J. Appl. Phys., Part 2 **33**, L804 (1994).
[10] A. Melzer, T. Trottenberg, and A. Piel, Phys. Lett. A **191**, 301 (1994).
[11] P. Epstein, Phys. Rev. **23**, 710 (1924).
[12] J. B. Pieper and J. Goree, Phys. Rev. Lett. **77**, 3137 (1996).
[13] A. Homann *et al.*, Phys. Lett. A **242**, 173 (1998).
[14] S. Nunomura, D. Samsonov, and J. Goree, Phys. Rev. Lett. **84**, 5141 (2000).
[15] T. Misawa *et al.*, Phys. Rev. Lett. **86**, 1219 (2001).
[16] P. K. Kaw and A. Sen, Phys. Plasmas **5**, 3552 (1998).
[17] G. Kalman, M. Rosenberg, and H. E. DeWitt, Phys. Rev. Lett. **84**, 6030 (2000).
[18] H. Ohta and S. Hamaguchi, Phys. Rev. Lett. **84**, 6026 (2000).
[19] F. M. Peeters and X. G. Wu, Phys. Rev. A **35**, 3109 (1987).
[20] F. Melandsø, Phys. Plasmas **3**, 3890 (1996).
[21] S. V. Vladimirov, P. V. Shevchenko, and N. F. Cramer, Phys. Rev. E **56**, R74 (1997).
[22] D. H. E. Dubin, Phys. Plasmas **7**, 3895 (2000).
[23] D. Samsonov, J. Goree, H. M. Thomas, and G. E. Morfill, Phys. Rev. E **61**, 5557 (2000).
[24] R. A. Quinn *et al.*, Phys. Rev. E **53**, R2049 (1996).
[25] U. Konopka, G. E. Morfill, and L. Ratke, Phys. Rev. Lett. **84**, 891 (2000).
[26] U. Konopka, Doctorate thesis, Ruhr-Universität-Bochum, Germany, 2000, pp. 48 and 49.
[27] T. Nitter, T. K. Aslaksen, F. Melandsdø, and O. Havnes, IEEE Trans. Plasma Sci. **22**, 159 (1994).
[28] S. Nunomura, T. Misawa, N. Ohno, and S. Takamura, Phys. Rev. Lett. **83**, 1970 (1999).
[29] A. V. Ivlev, U. Konopka, and G. Morfill, Phys. Rev. E **62**, 2739 (2000).